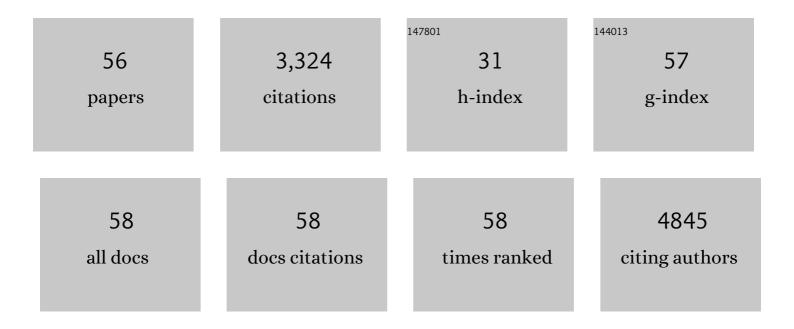
## Kai Pan

## List of Publications by Year in descending order

Source: https://exaly.com/author-pdf/3331159/publications.pdf Version: 2024-02-01



ΚΛΙ ΡΛΝ

#	Article	IF	CITATIONS
1	Monodisperse MnO nanoparticles in situ grown on reduced graphene oxide via hydrophobic interaction for excellent electromagnetic wave absorption. Journal of Materials Research, 2022, 37, 2175-2184.	2.6	3
2	Review on Lowâ€Cost Counter Electrode Materials for Dye‧ensitized Solar Cells: Effective Strategy to Improve Photovoltaic Performance. Advanced Materials Interfaces, 2022, 9, .	3.7	35
3	Surface engineering of mesoporous anatase titanium dioxide nanotubes for rapid spatial charge separation on horizontal-vertical dimensions and efficient solar-driven photocatalytic hydrogen evolution. Journal of Colloid and Interface Science, 2021, 586, 75-83.	9.4	25
4	Cadmium sulfide quantum dots/dodecahedral polyoxometalates/oxygen-doped mesoporous graphite carbon nitride with Z-scheme and Type-II as tandem heterojunctions for boosting visible-light-driven photocatalytic performance. Journal of Colloid and Interface Science, 2021, 582, 752-763.	9.4	39
5	Facile in-situ fabrication of nanocoral-like bimetallic Co-Mo carbide/nitrogen-doped carbon: a highly active and stable electrocatalyst for hydrogen evolution. Journal of Materials Science, 2021, 56, 11894-11906.	3.7	3
6	Zinc sulfide quantum dots/zinc oxide nanospheres/bismuth-enriched bismuth oxyiodides as Z-scheme/type-II tandem heterojunctions for an efficient charge separation and boost solar-driven photocatalytic performance. Journal of Colloid and Interface Science, 2021, 592, 259-270.	9.4	35
7	Plasma Cu-decorated TiO2â^'x/CoP particle-level hierarchical heterojunctions with enhanced photocatalytic-photothermal performance. Journal of Hazardous Materials, 2021, 414, 125487.	12.4	36
8	Hierarchical CoP Nanostructures on Nickel Foam as Efficient Bifunctional Catalysts for Water Splitting. ChemSusChem, 2021, 14, 1094-1102.	6.8	20
9	Engineering oxygen vacancies in CoO@Co <sub>3</sub> O <sub>4</sub> /C nanocomposites for enhanced electrochemical performances. Nanoscale, 2021, 13, 19518-19526.	5.6	17
10	Dual plasmons-promoted electron-hole separation for direct Z-scheme Bi3O4Cl/AgCl heterojunction ultrathin nanosheets and enhanced photocatalytic-photothermal performance. Journal of Hazardous Materials, 2020, 384, 121268.	12.4	34
11	Surface domain heterojunction on rutile TiO <sub>2</sub> for highly efficient photocatalytic hydrogen evolution. Nanoscale Horizons, 2020, 5, 1596-1602.	8.0	15
12	Hollow Octahedral Cu <sub>2–<i>x</i></sub> S/CdS/Bi <sub>2</sub> S <sub>3</sub> p–n–p Type Tandem Heterojunctions for Efficient Photothermal Effect and Robust Visible-Light-Driven Photocatalytic Performance. ACS Applied Materials & Interfaces, 2020, 12, 40328-40338.	8.0	77
13	Monodispersed Nickel Phosphide Nanocrystals in Situ Grown on Reduced Graphene Oxide with Controllable Size and Composition as a Counter Electrode for Dye-Sensitized Solar Cells. ACS Sustainable Chemistry and Engineering, 2020, 8, 5920-5926.	6.7	27
14	Engineering surface defects on two-dimensional ultrathin mesoporous anatase TiO <sub>2</sub> nanosheets for efficient charge separation and exceptional solar-driven photocatalytic hydrogen evolution. Journal of Materials Chemistry C, 2020, 8, 3476-3482.	5.5	34
15	Facet-Dependent SnS Nanocrystals as the High-Performance Counter Electrode Materials for Dye-Sensitized Solar Cells. ACS Sustainable Chemistry and Engineering, 2019, 7, 14353-14360.	6.7	11
16	Surface-defect-rich mesoporous NH2-MIL-125 (Ti)@Bi2MoO6 core-shell heterojunction with improved charge separation and enhanced visible-light-driven photocatalytic performance. Journal of Colloid and Interface Science, 2019, 554, 324-334.	9.4	44
17	Surface-oxygen vacancy defect-promoted electron-hole separation of defective tungsten trioxide ultrathin nanosheets and their enhanced solar-driven photocatalytic performance. Journal of Colloid and Interface Science, 2019, 557, 18-27.	9.4	14
18	Carbon nanotubes <i>in situ</i> embedded with NiS nanocrystals outperform Pt in dye-sensitized solar cells: interface improved activity. Journal of Materials Chemistry A, 2019, 7, 10405-10411.	10.3	40

Kai Pan

#	Article	IF	CITATIONS
19	Plasmon Ag and CdS quantum dot co-decorated 3D hierarchical ball-flower-like Bi <sub>5</sub> O <sub>7</sub> I nanosheets as tandem heterojunctions for enhanced photothermal–photocatalytic performance. Catalysis Science and Technology, 2019, 9, 6714-6722.	4.1	29
20	Surface Plasmon Resonanceâ€Enhanced Visibleâ€NIRâ€Driven Photocatalytic and Photothermal Catalytic Performance by Ag/Mesoporous Black TiO <sub>2</sub> Nanotube Heterojunctions. Chemistry - an Asian Journal, 2019, 14, 177-186.	3.3	39
21	Flower-like CoP microballs assembled with (002) facet nanowires via precursor route: Efficient electrocatalysts for hydrogen and oxygen evolution. Electrochimica Acta, 2018, 259, 830-840.	5.2	33
22	Morphology Effect of NiSe Hierarchical Microspheres on the Performance of Dye-Sensitized Solar Cells. ACS Applied Nano Materials, 2018, 1, 4900-4909.	5.0	18
23	Surface defect-mediated efficient electron-hole separation in hierarchical flower-like bismuth molybdate hollow spheres for enhanced visible-light-driven photocatalytic performance. Journal of Colloid and Interface Science, 2018, 531, 664-671.	9.4	25
24	Flowerâ€Like Nickel Phosphide Microballs Assembled by Nanoplates with Exposed Highâ€Energy (O O 1) Facets: Efficient Electrocatalyst for the Hydrogen Evolution Reaction. ChemSusChem, 2017, 10, 4899-4908.	6.8	55
25	High Catalytic Activity of W <sub>18</sub> O <sub>49</sub> Nanowire-Reduced Graphite Oxide Composite Counter Electrode for Dye-Sensitized Solar Cells. ChemistrySelect, 2017, 2, 8927-8935.	1.5	12
26	Selenization of Cu <sub>2</sub> ZnSnS <sub>4</sub> Enhanced the Performance of Dye-Sensitized Solar Cells: Improved Zinc-Site Catalytic Activity for I <sub>3</sub> <sup>–</sup> . ACS Applied Materials & Interfaces, 2017, 9, 37662-37670.	8.0	33
27	Hexagonal FeS nanosheets with high-energy (001) facets: Counter electrode materials superior to platinum for dye-sensitized solar cells. Nano Research, 2016, 9, 2862-2874.	10.4	38
28	Bifunctional Ag/Fe/N/C Catalysts for Enhancing Oxygen Reduction via Cathodic Biofilm Inhibition in Microbial Fuel Cells. ACS Applied Materials & amp; Interfaces, 2016, 8, 6992-7002.	8.0	78
29	Large-scale synthesis of stable mesoporous black TiO <sub>2</sub> nanosheets for efficient solar-driven photocatalytic hydrogen evolution via an earth-abundant low-cost biotemplate. RSC Advances, 2016, 6, 50506-50512.	3.6	29
30	Black N/Hâ€TiO <sub>2</sub> Nanoplates with a Flowerâ€Like Hierarchical Architecture for Photocatalytic Hydrogen Evolution. ChemSusChem, 2016, 9, 2841-2848.	6.8	73
31	Facile Strategy to Fabricate Uniform Black TiO <sub>2</sub> Nanothorns/Graphene/Black TiO <sub>2</sub> Nanothorns Sandwichlike Nanosheets for Excellent Solarâ€Driven Photocatalytic Performance. ChemCatChem, 2016, 8, 3240-3246.	3.7	21
32	Controlled synthesis of CaTiO <sub>3</sub> :Ln <sup>3+</sup> nanocrystals for luminescence and photocatalytic hydrogen production. RSC Advances, 2016, 6, 5761-5766.	3.6	22
33	Pure phase orthorhombic MgTi <sub>2</sub> O <sub>5</sub> photocatalyst for H <sub>2</sub> production. RSC Advances, 2015, 5, 106151-106155.	3.6	22
34	Fe <sub>3</sub> W <sub>3</sub> C/WC/Graphitic Carbon Ternary Nanojunction Hybrids for Dye‧ensitized Solar Cells. ChemSusChem, 2015, 8, 726-733.	6.8	16
35	A novel Fe <sub>3</sub> C/graphitic carbon composite with electromagnetic wave absorption properties in the C-band. RSC Advances, 2015, 5, 60135-60140.	3.6	45
36	In situ synthesis of a NiS/Ni <sub>3</sub> S <sub>2</sub> nanorod composite array on Ni foil as a FTO-free counter electrode for dye-sensitized solar cells. Nanoscale, 2015, 7, 1623-1626.	5.6	94

Kai Pan

#	Article	IF	CITATIONS
37	Fabrication of noncovalently functionalized brick-like β-cyclodextrins/graphene composite dispersions with favorable stability. RSC Advances, 2014, 4, 2813-2819.	3.6	14
38	Composites of small Ag clusters confined in the channels of well-ordered mesoporous anatase TiO2 and their excellent solar-light-driven photocatalytic performance. Nano Research, 2014, 7, 731-742.	10.4	102
39	A Floating Porous Crystalline TiO <sub>2</sub> Ceramic with Enhanced Photocatalytic Performance for Wastewater Decontamination. European Journal of Inorganic Chemistry, 2013, 2013, 2411-2417.	2.0	59
40	Hierarchical flake-like Bi2MoO6/TiO2 bilayer films for visible-light-induced self-cleaning applications. Journal of Materials Chemistry A, 2013, 1, 6961.	10.3	102
41	Hierarchical Composite of Ag/AgBr Nanoparticles Supported on Bi <sub>2</sub> MoO <sub>6</sub> Hollow Spheres for Enhanced Visible‣ight Photocatalytic Performance. ChemPlusChem, 2013, 78, 117-123.	2.8	58
42	Highly crystalline graphene/carbon black composite counter electrodes with controllable content: Synthesis, characterization and application in dye-sensitized solar cells. Electrochimica Acta, 2013, 96, 155-163.	5.2	59
43	Confinement Effect on Ag Clusters in the Channels of Wellâ€Ordered Mesoporous TiO <sub>2</sub> and their Enhanced Photocatalytic Performance. ChemCatChem, 2013, 5, 1354-1358.	3.7	13
44	Facile Synthesis of High-Crystallinity Graphitic Carbon/Fe <sub>3</sub> C Nanocomposites As Counter Electrodes for High-Efficiency Dye-Sensitized Solar Cells. ACS Applied Materials & Interfaces, 2013, 5, 3663-3670.	8.0	127
45	A facile and green synthesis route towards two-dimensional TiO2@Ag heterojunction structure with enhanced visible light photocatalytic activity. CrystEngComm, 2013, 15, 5821.	2.6	25
46	Highly dispersed Ni-decorated porous hollow carbon nanofibers: fabrication, characterization, and NOx gas sensors at room temperature. Journal of Materials Chemistry, 2012, 22, 24814.	6.7	35
47	Controlled synthesis of thorny anatase TiO <sub>2</sub> tubes for construction of Ag–AgBr/TiO <sub>2</sub> composites as highly efficient simulated solar-light photocatalyst. Journal of Materials Chemistry, 2012, 22, 2081-2088.	6.7	84
48	Room temperature solution synthesis of hierarchical bow-like Cu2O with high visible light driven photocatalytic activity. RSC Advances, 2012, 2, 2875.	3.6	38
49	Facile preparation of porous NiTiO3 nanorods with enhanced visible-light-driven photocatalytic performance. Journal of Materials Chemistry, 2012, 22, 16471.	6.7	176
50	Fabrication of Rice‣ike Porous Anatase TiO <sub>2</sub> with High Thermal Stability and Enhanced Photocatalytic Performance. ChemCatChem, 2012, 4, 844-850.	3.7	17
51	Fabrication of a 3D Hierarchical Flower‣ike MgO Microsphere and Its Application as Heterogeneous Catalyst. European Journal of Inorganic Chemistry, 2012, 2012, 954-960.	2.0	27
52	Facile solvothermal synthesis of hierarchical flower-like Bi <sub>2</sub> MoO <sub>6</sub> hollow spheres as high performance visible-light driven photocatalysts. Journal of Materials Chemistry, 2011, 21, 887-892.	6.7	427
53	3D hierarchical flower-like TiO2 nanostructure: morphology control and its photocatalytic property. CrystEngComm, 2011, 13, 2994.	2.6	237
54	Wellâ€Ordered Largeâ€Pore Mesoporous Anatase TiO <sub>2</sub> with Remarkably High Thermal Stability and Improved Crystallinity: Preparation, Characterization, and Photocatalytic Performance. Advanced Functional Materials, 2011, 21, 1922-1930.	14.9	431

#	Article	IF	CITATIONS
55	Solvothermal Synthesis, Characterization, and Formation Mechanism of a Singleâ€Layer Anatase TiO <sub>2</sub> Nanosheet with a Porous Structure. European Journal of Inorganic Chemistry, 2011, 2011, 754-760.	2.0	22
56	Assembly of β-Cyclodextrins Acting as Molecular Bricks onto Multiwall Carbon Nanotubes. Journal of Physical Chemistry C, 2008, 112, 951-957.	3.1	72